PHYSICAL REVIEW B **66**, 155110 (2002)

Electron momentum density in yttrium

G. Kontrym-Sznajd, M. Samsel-Czekała, and A. Pietraszko
W. Trzebiatowski Institute of Low Temperature and Structure Research, Polish Academy of Sciences,
P.O. Box 1410, 50-950 Wrocław 2, Poland

H. Sormann
Institut für Theoretische Physik, Technische Universität Graz, Petersgasse 16, A-8010 Graz, Austria

S. Manninen, S. Huotari, K. Hämäläinen, and J. Laukkanen
Division of X-ray Physics, Department of Physical Sciences, University of Helsinki,
P.O. Box 64, FIN–00014 University of Helsinki, Finland

R. N. West
Department of Physics, University of Texas at Arlington, P.O. Box 19059, Arlington, Texas 76019

W. Schülke
Institute of Physics, University of Dortmund, P.O. Box. 217, D-44221 Dortmund, Germany

(Received 8 April 2002; revised manuscript received 30 July 2002; published 23 October 2002)

A simultaneous analysis of high-resolution directional Compton profiles and two-dimensional angular correlation of positron annihilation experimental data has been performed by studying both a directional anisotropy of measured spectra and reconstructed densities. The results were compared with theoretical fully relativistic augmented plane-wave calculations with and without including correlation effects. Estimated symmetry selection rules have allowed us to establish some values of Fermi momenta. Both experiments show exactly the same shape of the anisotropy of the momentum densities, in agreement with the band structure results. In the positron annihilation data electron-positron correlations are not seen while in both experiments electron-electron correlations are observed.

DOI: 10.1103/PhysRevB.66.155110 PACS number(s): 71.18.+y, 74.25.Jb, 13.60.Fz, 78.70.Bj

I. INTRODUCTION

The electronic structure of yttrium [$4d$ transition metal with the hexagonal close-packed, (hcp) structure] is similar to that of trivalent heavier rare earths in their paramagnetic phases. According to all theoretical calculations,[1–6] except Ref. 2, the first two valence bands are fully occupied and there are two Fermi surfaces (FS's) in the third and fourth bands.

The electronic structure of Y has been studied by measuring one-dimensional angular correlation of annihilation radiation (1D ACAR) spectra representing plane projections of the electron-positron (e-p) momentum density $\rho(\mathbf{p})$,[7–9] 2D ACAR spectra [line projections of $\rho(\mathbf{p})$],[10,11] and the de Haas–van Alphen (dHvA) effect.[12] All these experimental results agree well with calculations by Loucks.[1] The interpretation of 2D ACAR data in terms of $\rho(\mathbf{k})$ [reconstructed densities folded into the first Brillouin zone (BZ) (Ref. 13)], gives the average FS's of Y (Ref. 10) with precise information about the shape and size of its *webbing* feature. On the other hand, the interpretation of the same data in terms of $\rho(\mathbf{p})$ gives two FS's in separate bands.[11]

In this work we present the electron momentum density $\rho(\mathbf{p})$ reconstructed from 12 high-resolution directional Compton profiles (CP's), compared with electron-positron (e-p) momentum density reconstructed from the 2D ACAR spectra[10,11] and corresponding theoretical results. We show how the knowledge of $\rho(\mathbf{p})$ in the whole $\mathbf{p}$ space allows us to extract dimensions of the FS's in different bands via so-called symmetry selection rules.[14]

The experimental CP's were measured using 60 keV x rays and an overall resolution (i.e., geometrical and energetic) of 0.16 atomic units of momentum (a.u.) at the European Synchrotron Radiation Facility (ESRF), France. Positron annihilation spectra were measured with similar overall resolution (of approximately 0.15 a.u.) using the 2D ACAR spectrometer at the University of Texas at Arlington.[10]

Reconstruction techniques, applied to both plane and line projections of 3D density and described shortly in the next section, are based on the solution of the Radon transform in terms of orthogonal polynomials.[15,16] The theoretical $\rho(\mathbf{p})$ was obtained from fully relativistic augmented plane-wave (APW) band structure calculations both for electron and e-p pair wave functions within independent particle models and after including correlation effects.

II. APPLIED TECHNIQUES

A. Experiments

In a Compton scattering experiment one measures plane projections of the electron density in the extended zone ($\mathbf{p}$ space):

$$J(p_z)=\int_{-\infty}^{\infty}\int_{-\infty}^{\infty}dp_x dp_y \rho(\mathbf{p}). \tag{1}$$

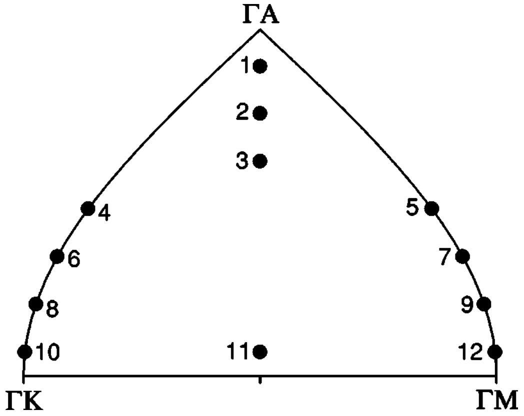

FIG. 1. Special directions (marked by numbered dots) in the nonequivalent part of the hcp BZ—12 orientations of p_z along which CP's were measured.

The experiment for Y was carried out for 12 sample orientations with p_z along directions described in the spherical system by angles (Θ,φ): $1\equiv(9.5,15)$, $2\equiv(21.8,15)$, $3\equiv(34.2,15)$, $4\equiv(46.6,0)$, $5\equiv(46.6,30)$, $6\equiv(59,0)$, $7\equiv(59,30)$, $8\equiv(71.4,0)$, $9\equiv(71.4,30)$, $10\equiv(83.8,0)$, $11\equiv(83.8,15)$, and $12\equiv(83.8,30)$ (special symmetry directions[17]) where angles are given in degrees; see Fig. 1. Owing to such a choice of directions p_z as many lattice harmonics as the number of measured spectra can be fitted (without undue loss of precision) to the spectra.[17]

The original single crystals for the experiment were provided by the University of Birmingham (U.K.). Samples used in the experiment were cut from the original crystal pieces according to the desired directions using the four-circle fully automatic x-ray diffractometer (orientation with accuracy $\pm 0.05°$). The oriented sample with a goniometer head was mounted on a wire saw and then was cut with accuracy $\pm 0.5°$. In order to avoid uncertainties in the absorption and multiple-scattering corrections all samples had an identical shape of a bar with a height of about 5 mm and a cross section of a square with a side of 1 mm.

The Compton scattering experiments were performed at the beamline ID15B of the European Synchrotron Radiation Facility (ESRF, Grenoble, France).[18] Incident photons from an asymmetric multipole wiggler source were monochromatized ($E_1 = 55.8$ keV) with a bent Si crystal using the (311) reflection. The photon beam was confined to dimensions of 4 mm (height)$\times$0.3 mm (width) at the sample position. Almost the full size of the sample could be then utilized, and the same geometry guarantees that any error in the absorption or multiple-scattering correction cancels out when the differences in the Compton profiles are considered. The spectrum of the scattered photons was recorded with a scanning crystal spectrometer, the analyzer crystal and reflection being Ge(440) in a scattering angle of 173°. The analyzed photons were detected by a NaI scintillation detector. The distance between the experimental points was equal to about 0.03 a.u. of momentum, while the resolution of the equipment was about 0.16 a.u. A total of $\sim$150 000 counts was collected at the Compton peak of each profile (core+valence), yielding statistical accuracy of 2.6% at $p_z=0$ of the valence profile. The spectra were corrected for absorption in the sample and in the air path and the efficiency of both the analyzer crystal and the detector. A linear background was subtracted from the spectra using the fact that the Compton profile has to reach pure core contribution ($2s$-$4p$) at high absolute momenta; note that the $1s$ binding energy is larger than our energy transfer. The intensity of the incident photon beam was monitored using a Si PIN diode, and the Compton spectra were normalized to the monitor current. All Compton profiles were normalized to three valence electrons ($4d^1 5s^2$).

Two-dimensional ACAR spectra which represent line projections of the e-p density in the extended zone (**p** space),

$$J(p_y,p_z)=\int_{-\infty}^{\infty} dp_x \rho(\mathbf{p}), \tag{2}$$

were measured for five directions p_x, which changed by 7.5° intervals from the direction ΓM to ΓK.[10] Each spectrum was determined for 258$\times$258 points (p_y,p_z) in the interval $|p_i| \leqslant 2.5$ a.u. with a total number of counts for each projection $\sim 9\times 10^7$. Following the usual processing of the measured spectra, i.e., correcting for the momentum sampling function arising from a finite size of detectors (raw data) (Ref. 19)—a "maximum entropy algorithm" was applied to each raw spectrum (deconvoluted spectra).[20] The strength of the procedure is that it does not introduce artifacts into the data. We have similar experience with another deconvolution algorithm.[21]

B. Reconstruction techniques

For the reconstruction of 3D electron momentum densities from CP's, the Jacobi polynomials reconstruction technique[15] was applied. Measured spectra were expanded into the hcp lattice harmonics $F_{l\nu}(\Theta,\varphi)$:

$$J(p_z)\equiv J_{\Theta,\varphi}(p)=\sum_{l\nu} g_{l\nu}(p)F_{l\nu}(\Theta,\varphi), \tag{3}$$

where

$$F_{l\nu}=\sqrt{\frac{(2l+1)}{4\pi}}P_l(\cos\Theta)$$

or

$$\sqrt{\frac{(2l+1)(l-|m|)!}{2\pi(l+|m|)!}}P_l^{|m|}(\cos\Theta)\cos(m\varphi)$$

for $l=2i$ and $l=6+2i$ (left and right expressions for $F_{l\nu}$, respectively) with $m=6+6i$ and $m\leqslant l$ $(i=0,1,2,3,\dots)$. $P_l^{|m|}$ are associated Legendre polynomials, and the index ν distinguishes harmonics of the same order *l*. Here (Θ,φ) represent the azimuthal and polar angles of the instrumental p_z axis with respect to the coordinate system of the reciprocal lattice.

The radial functions $g_{l\nu}(p)$ (in the unit system $0\leqslant p\leqslant 1$) are expanded into the Jacobi polynomials $P_n^{(1,1)}$,

$$g_{l\nu}(p)=\sum_{k=0}^{\infty} a_{l\nu k}(1-p^2)P_{l+2k}^{(1,1)}(p), \tag{4}$$

and the coefficients $a_{l\nu k}$ are evaluated by using the orthogonality relation for $P_n^{(1,1)}$:

$$a_{l\nu k}=\frac{(l+2k+2)(2l+4k+3)}{4(l+2k+1)}\int_0^1 g_{l\nu}(p)P_{l+2k}^{(1,1)}(p)dp. \tag{5}$$

Next, radial parts of the density are obtained,

$$\rho_{l\nu}(p)=\frac{1}{\pi}\sum_{k=0}^{\infty} a_{l\nu k}(1+2k+l)p^l P_k^{(0,l+1/2)}(2p^2-1), \tag{6}$$

where values of the Jacobi polynomials are calculated from their recurrence relation:

$$P_0^{(\alpha,\beta)}(x)=1, \quad P_1^{(\alpha,\beta)}(x)=[(\alpha+\beta+2)x+\alpha-\beta]/2,$$

$$\begin{aligned}2(n+1)(n+\alpha+\beta+1)(2n+\alpha+\beta)P_{n+1}^{(\alpha,\beta)}(x)\\ =(2n+\alpha+\beta+1)[\alpha^2-\beta^2+(2n+\alpha+\beta)\\ \times(2n+\alpha+\beta+2)x]P_n^{(\alpha,\beta)}(x)\\ -2(n+\alpha)(n+\beta)(2n+\alpha+\beta+2)P_{n-1}^{(\alpha,\beta)}(x).\end{aligned}$$

Finally, $\rho(\mathbf{p})$ is derived from its expansion into the lattice harmonics:

$$\rho(\mathbf{p})=\sum_{l\nu} \rho_{l\nu}(p)F_{l\nu}(\Theta,\varphi). \tag{7}$$

For the reconstruction of 3D electron-positron momentum densities from 2D ACAR spectra Cormack's technique[16] was applied. Here reconstruction of the 3D density is reduced to sets of reconstructions of 2D densities, performed independently on parallel planes $p_z=\text{const}$, perpendicular to the sixfold rotation axis. In such a case lattice harmonics reduce to a cosine series and on each of planes $p_z=\text{const}$ we have independent 2D quantities:

$$\rho(\mathbf{p})\equiv\rho(p,\Theta)=\sum_{m=0}^{\infty} \rho_m(p)\cos(m\Theta), \tag{8}$$

$$J(p_y,p_z=\text{const})\equiv J(p,\varphi)=\sum_{m=0}^{\infty} J_m(p)\cos(m\varphi), \tag{9}$$

with $m=6+6i$.

In 1964 Cormack showed that if $J_m(p)$ is expanded into a series of Chebyshev polynomials of the second kind $[U_l(p)]$,

$$J_m(p)=2\sum_k^{\infty} a_m^k\sqrt{1-p^2}U_{m+2k}(p), \tag{10}$$

then Eq. (2) can be solved analytically and

$$\rho_m(p)=\sum_k^{\infty} (m+2k+1)a_m^k R_m^k(p), \tag{11}$$

where $R_m^k(p)$ are Zernike polynomials and

$$a_m^k=\frac{1}{\pi}\int_{-1}^1 J_m(p)U_{m+2k}(p)dp. \tag{12}$$

The last equation is given in the unit system $0\leqslant p\leqslant 1$.

Both reconstruction techniques are based on the same solution of the Radon transform in the N-dimensional space $\mathcal{R}^N$ given in terms of the orthogonal Gegenbauer polynomials; for more details see the Appendix.

C. Theoretical momentum densities

Electron-positron momentum densities in the **p** space are given by the following relation:

$$\rho(\mathbf{p})\simeq\sum_j n_{\mathbf{k}j}\left|\int_{-\infty}^{\infty} e^{-i\mathbf{p}\cdot\mathbf{r}}\psi_{\mathbf{k}j}^{e\text{-}p}(\mathbf{r},\mathbf{r})d\mathbf{r}\right|^2, \tag{13}$$

where $\psi^{e\text{-}p}$ means the pair wave function. $n_{\mathbf{k}j}$ is the occupation number (0,1) of an electron in the initial state $\mathbf{k}j$. We used the following models for $\psi_{\mathbf{k}j}^{e\text{-}p}(\mathbf{r},\mathbf{r})$:

(i) $\psi_{\mathbf{k}j}^{e-p}(\mathbf{r},\mathbf{r})=\psi_{\mathbf{k}j}(\mathbf{r})$—we consider only electron densities; i.e., the influence of the positron is completely neglected.

(ii) $\psi_{\mathbf{k}j}^{e-p}(\mathbf{r},\mathbf{r})=\psi_{\mathbf{k}j}(\mathbf{r})\psi_+(\mathbf{r})$—the independent particle model (IPM), where for the evaluation of the electron and thermalized positron wave functions, the fully relativistic APW method has been applied (for details, see Ref. 22).

(iii) The Coulombic interaction between the annihilating particles is described by various e-p interaction theories.[23] Among these theoretical approaches, state-independent local density approximations (LDA) and the Bloch-modified ladder (BML) theory give the best description of 2D ACAR experiments in Y.[23] We also obtained that in this metal (contrary to simple metals or transition metals as Cu), these theoretical results are very similar to IPM results, if we study the momentum dependence of the electron-positron momentum density, not its absolute value. For this reason, we shall henceforth present only IPM results.

(iv) The influence of e-e correlations (for Compton profiles) was taken into account following the work of Cardwell and Cooper[24] based on the proposal of Lam and Platzman,[25] where the Lam-Platzman corrections have been calculated from the self-consistent APW electron charge density.

Theoretical densities were calculated along ΓM and ΓK directions on planes Pi perpendicular to the hexagonal c axis and distant $1/2|\Gamma A|$ [the plane Pi is situated $(i-1)\times 0.145\,05$ a.u. above the ΓMK plane]. The resulting Fermi surface is very similar to theoretical results by Loucks (see Fig. 2).

III. RESULTS AND DISCUSSION

We would like to point out that in the case of our data there are no errors in reconstructed densities connected with a truncation of infinite series [Eqs. (3) and (9)] because of a

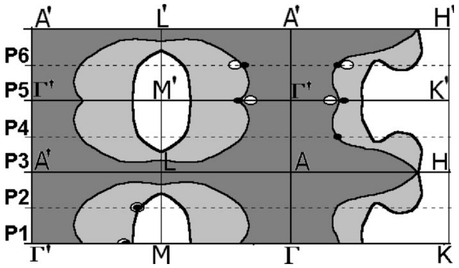

FIG. 2. Theoretical Fermi surface in Y, in the repeated zone scheme, derived from Loucks (Ref. 1). Electrons in the fourth and holes in the third zones are marked by white and dark grey colors, respectively. Values of $\mathbf{p}_F$ for which theoretical $\rho(\mathbf{p})$ have jumps are marked by black dots and corresponding values of $\mathbf{p}_F$ obtained from reconstructed *e-p* densities by open circles (Ref. 11). The distance $|\Gamma K| = 0.6077$ a.u. and $|\Gamma M| = 0.5263$ a.u.

finite number of measured spectra. Namely, for 2D spectra $J(p_y, p_z)$ we performed a reconstruction on each plane Pi independently, having five projections $J(p_y, p_z = \text{const})$ for different orientations of p_y. For deconvoluted 2D ACAR data, densities reconstructed from five projections [harmonics with $\cos(24\varphi)$] are the same (in detail) as derived from four projections [harmonics with $\cos(18\varphi)$]. Even three projections [harmonics with $\cos(12\varphi)$], which are quite sufficient for raw data, describe densities well. The measurement of five 2D ACAR spectra is equivalent to measuring at least 35 (up to 45) CP's and for three 2D ACAR data the corresponding number of CP's equals 12 (up to 18). Tests, performed for 1D profiles, created from deconvoluted 2D ACAR spectra, showed that a measurement of 12 CP's for special orientations of p_z could allow to reproduce densities [within the experimental full width at half maximum (FWHM)] properly; see Fig. 3.

For the sake of the variety of theoretical and experimental results in the further part of the paper we will use the following symbols (also for electron or *e-p* momentum densities, reconstructed from the corresponding spectra): EMD, theoretical electron momentum densities without *e-e* correlations corrections; LP, theoretical electron momentum densities with the Lam-Platzman correction;[24] IPM, theoretical *e-p* momentum densities without *e-e* and *e-p* correlation corrections; CP and CPc, raw experimental and convoluted theoretical Compton profiles; and raw and dec, raw and deconvoluted 2D ACAR spectra.

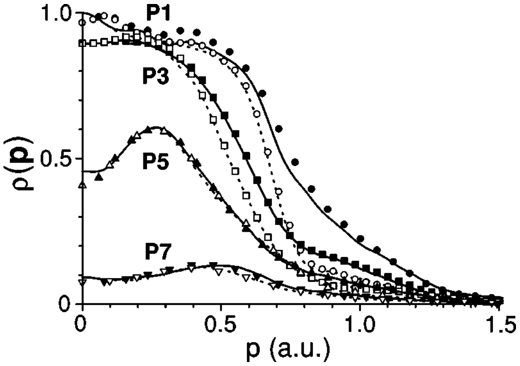

FIG. 3. *e-p* momentum densities in Y reconstructed from 12 $J(p_z)$ profiles (for p_z marked in Fig. 1) created from deconvoluted 2D ACAR spectra, compared with "model" (densities reconstructed from five 2D ACAR profiles). Results displayed along ΓK and ΓM directions are marked by solid and dashed lines for the "model" and by solid and open symbols for reconstructed densities.

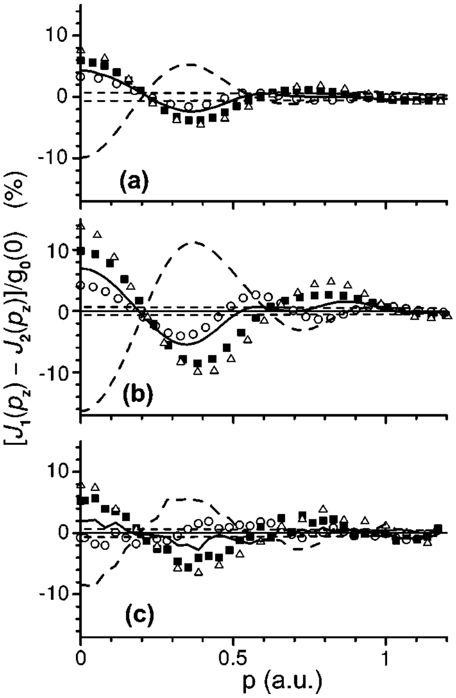

FIG. 4. Directional anisotropy of 1D profiles in Y: $J_1(p_z) - J_2(p_z)$ for directions (marked in Fig. 1): (5,4), open circles; (7,6), solid lines; (9,8), black squares; (12,10), open triangles; (11,1), thick dashed lines. Parts (a), (b), and (c) display differences between; 1D profiles calculated from raw 2D ACAR spectra and theoretical convoluted and experimental CP's, respectively. Thin dashed lines mark the total experimental error for CP's. All in % of the average value of $J(p_z = 0)$.

What concerns the Compton profiles, the *e-e* correlation causes a part of the electron momentum density to move from low to high momenta[26–31] when compared to IPM results. For the alloy $Cu_{0.9}Al_{0.1}$ (Ref. 26) and also for other materials (see, e.g., Refs. 27 and 28), the differences between experimental and theoretical directional CPs, $J^{CP}(p_z) - J^{CPc}(p_z)$, were found to be almost the same in each direction, with a shape similar to the isotropic Lam-Platzman correction. This momentum transfer is also characteristic for a homogeneous electron gas where *e-e* correlations are theoretically described according to Daniel and Vosko and other authors.[32–36] Contrary to $Cu_{0.9}Al_{0.1}$, the correlation effects in Y are seen to be strongly anisotropic. This is visible in Fig. 4, where the anisotropy of experimental CP's [Fig. 4(c)] is roughly a factor of 2 smaller than the anisotropy in convoluted theoretical CP's [see Fig. 4(b)].

Such a trend (smaller anisotropy in momentum space) is often observed if electronic systems of significant spatial anisotropy are studied by Compton scattering experiments (see, for example, Ref. 30). If we now consider the directional anisotropy of profiles obtained from 1D ACAR experiments

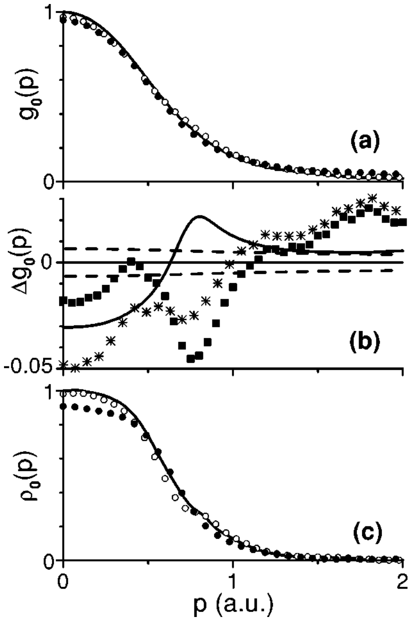

FIG. 5. Isotropic average of Compton profiles: convoluted g_0^{EMD} (solid line), convoluted g_0^{LP} and g_0^{CP} (open and solid circles, respectively), normalized to the same area—panel (a). Corresponding densities ρ_0 are displayed in panel (c). Panel (b) shows the differences $g_0^{LP}-g_0^{EMD}$ (solid line), $g_0^{CP}-g_0^{EMD}$ (stars), and $g_0^{CP}-g_0^{LP}$ (squares) on the background of the total experimental error, marked by dashed lines.

[Fig. 4(a)], we observe a striking qualitative *and quantitative* similarity of these results with the corresponding experimental CP's of Fig. 4(c). Even if we take into account that the differences between J_1-J_2 of the 1D ACAR spectra are renormalized with respect to a $g_0(0)$ which also contains the core contribution of the *e*-*p* annihilation rate, this behavior will not be strongly changed, due to the fact that this core contribution is essentially reduced by the positron. We therefore have to conclude that, in yttrium, both the electron momentum density and the *e*-*p* momentum density are strongly influenced by fermion-fermion correlations. This finding is surprising because almost all theoretical papers devoted to this question are based on the result of Carbotte and Kahana:[38] An annihilating *e*-*p* pair is, seen from outside, a neutral quantity with a strongly reduced coupling to its environment. Consequently, typical correlation effects as smearing at the Fermi momentum and high-momentum tails of the momentum distribution should be significantly smaller in *e*-*p* systems than in pure electron systems. This important point of our investigation will be further discussed in some detail in Sec. IV of this paper.

To examine the influence of *e*-*e* correlation effects on the electron momentum distribution in Y, in Fig. 5, we compare the isotropic average of experimental CP's and momentum densities [represented by the functions $g_0(p)$ and $\rho_0(p)$; see Eqs. (A3) and (A5), respectively] with corresponding theoretical results.

In Fig. 5(a) we display theoretically obtained values of g_0^{EMD} and g_0^{LP} (convoluted with the experimental resolution function) and g_0^{CP}, normalized to the same area. The differences between these curves are displayed in the panel (b), together with the experimental statistical uncertainty. The $\rho_0(p)$ reconstructed from the corresponding $g_0(p)$ are shown in Fig. 5(c). It can be seen from Fig. 5(b) that the Lam-Platzman correction is not adequate to describe the difference between the experimental and theoretical averages. Nevertheless, it shows a typical feature of *e*-*e* correlation effects in CP's, namely, a significant reduction of the momentum density at low momenta.

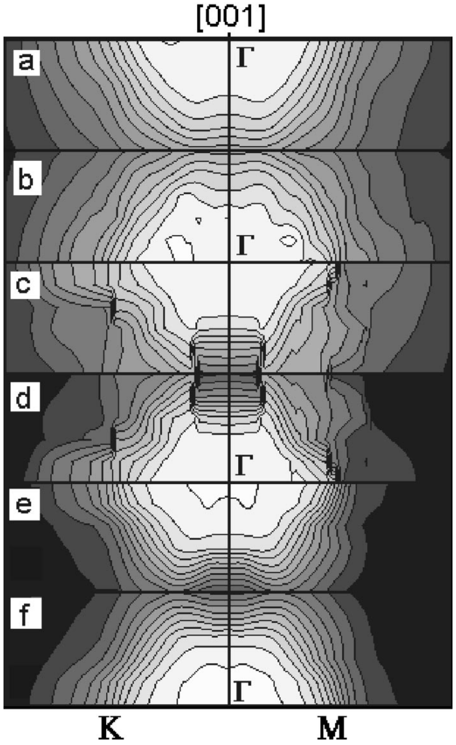

FIG. 6. Momentum densities in Y, containing the core contribution, along ΓK (left side) and ΓM (right side) and parallel directions, for momenta up to 1.37 a.u., on six planes P_i (up to 0.73 a.u.): (a) $\rho_{36}^{CP}(\mathbf{p})$, (b) $\rho_{60}^{CP}(\mathbf{p})$, (c) $\rho^{EMD}(\mathbf{p})$, (d) $\rho^{IPM}(\mathbf{p})$, (e) $\rho^{dec}(\mathbf{p})$, and (f) $\rho^{raw}(\mathbf{p})$. Densities range from 0 to 1 and the step size between two of 14 contour lines equals 0.077.

In Fig. 6 we present momentum densities reconstructed from CP's and 2D ACAR data in comparison to EMD and IPM results where these theoretical values are shown without correlation effects. In the case of the ACAR data, it was not possible to subtract the core contribution from the experimental spectra. Therefore, to compare densities measured in these two experiments, all momentum densities shown in Fig. 6 include this contribution.

As we can see from Figs. 6(c) and 6(d), the momentum dependence of ρ^{EMD} and ρ^{IPM} is similar, but the *e*-*p* momentum density contains an essentially smaller core contribution. This is caused by the repulsive interaction of the positron with the positive ions; due to this effect, the annihilation probability of the positron with highly localized core electrons is much smaller than the probability to annihilate with delocalized valence electrons. In Figs. 6(a) and 6(b), we also demonstrate how sensitively the densities $\rho^{CP}(\mathbf{p})$ depend on the number of the Jacobi polynomials used in the

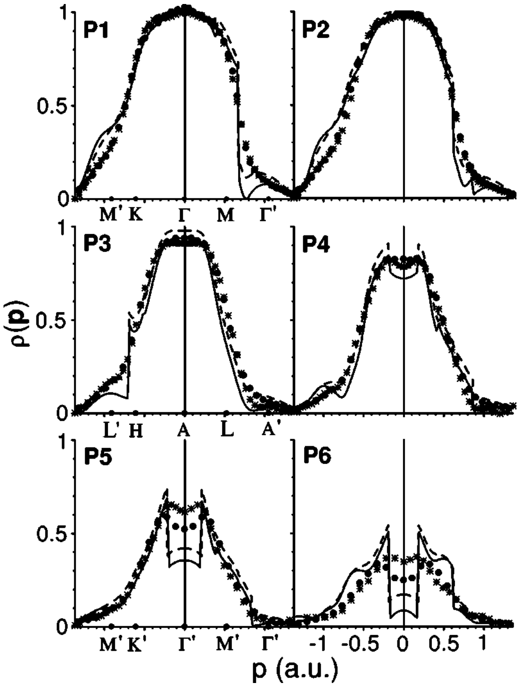

FIG. 7. Momentum densities in Y along ΓK and ΓM and parallel directions for $\rho^{EMD}(\mathbf{p})$ (solid lines), $\rho^{IPM}(\mathbf{p})$ (dashed lines), $\rho^{CP}(\mathbf{p})$ (stars), and $\rho^{raw}(\mathbf{p})$ (black dots).

reconstruction: ρ_{36}^{CP} and ρ_{60}^{CP} correspond to the use of polynomials up to the order 36 and 60, respectively.[37]

More detailed comparisons between theoretical and experimental results are given in Figs. 7–10. Because of the small contribution of the core electrons to the positron annihilation data, in all these figures, we show both the EMD and the densities reconstructed from CP's without their core contributions. Due to the experimental noise, results for densities reconstructed from CP's, $\rho^{CP}(\mathbf{p})$, are shown only for polynomials up to the order 36.[37] For this reason, certain details of $\rho(\mathbf{p})$, "seen" in the positron experiment (e.g., the holes around the Γ point in the planes $P5$ and $P6$ as can be

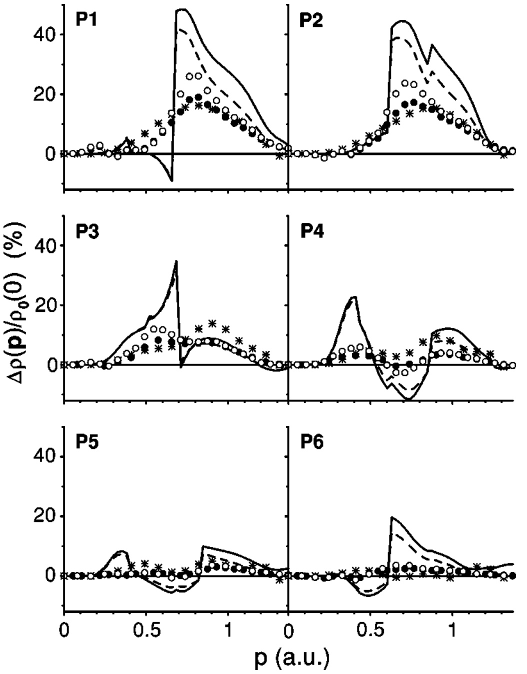

FIG. 8. Differences, in % of $\rho_0(0)$, between momentum densities along ΓK and ΓM for densities shown in Fig. 7 and for $\rho^{dec}(\mathbf{p})$ (open circles).

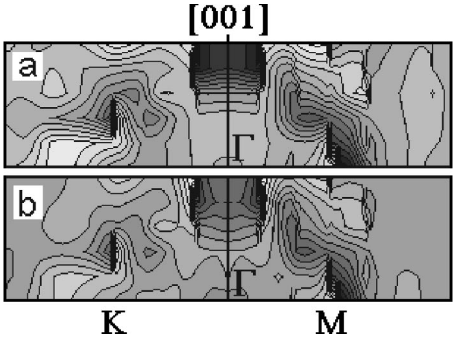

FIG. 9. Differences between theoretical and reconstructed densities in Y for $\rho^{EMD}(\mathbf{p})-\rho^{CP}(\mathbf{p})$ (a), $\rho^{IPM}(\mathbf{p})-\rho^{raw}(\mathbf{p})$ (b) and for the momentum range as in Fig. 6. The step size between two of 16 contour lines in each separate part equals, in % of $\rho_0(0)$, 3.7 (a), 3.4 (b), and the range of values is $\langle -36.5,18.8\rangle$, $\langle -27.2,23.9\rangle$, respectively.

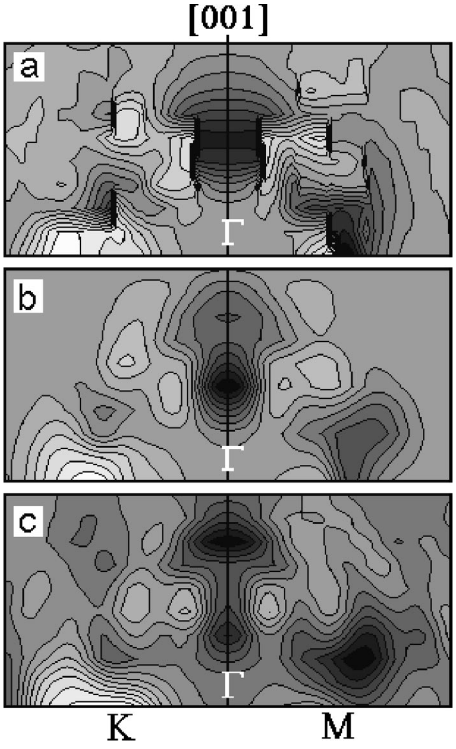

FIG. 10. Anisotropic part of electron momentum densities $\rho_a(\mathbf{p})$ in Y along ΓK and ΓM and parallel directions on ten planes Pi for pure theoretical EMD densities (a) and densities reconstructed from convoluted theoretical (b) and experimental (c) CP's for momenta up to 1.37 a.u. The step size between two of 16 contour lines in each separate part equals, in % of $\rho_0(0)$, 3.9 (a), 3.5 (b), and 1.7 (c), and the range of densities is $\langle -34.7,24.2\rangle$, $\langle -29.9,22\rangle$, and $\langle -11.8,13.4\rangle$, respectively.

observed in Figs. 3 and 7), are too smeared to appear in our Compton results.

To reproduce $\rho(\mathbf{p})$ properly it was necessary to get a proper shape of $J_1(p_z)-J_2(p_z)$ also for profiles (5,4) [see Fig. 4(c)]. Unfortunately the current experimental statistical accuracy is not adequate to produce these fine details. It must be noted, however, that in experimental Compton profiles all electrons equally contribute if the binding energy is smaller than the energy transfer. In the case of yttrium the number of valence electrons is $Z_{val}=3$ and the number of core electrons contributing in this experiment is $Z_{core}=34$ (recall that the 1s binding energy is larger than our energy transfer). Thus, in the total Compton profile, only 3/34 of the signal originates from the valence electrons. With a lower Z, the corresponding ratio is higher: For instance, for Be, the number of valence and core electrons is equal, which means significantly better relative statistical accuracy. Due to this fact and taking into account that reconstructed densities are smeared due to the finite experimental resolution, the agreement between theory and experiment is satisfactory. Moreover, the results displayed in Fig. 8 clearly point out that the deconvoluting procedure works well.

Figure 9 shows differences between corresponding theoretical and experimental densities $\rho^{EMD}(\mathbf{p})-\rho^{CP}(\mathbf{p})$ and $\rho^{IPM}(\mathbf{p})-\rho^{raw}(\mathbf{p})$, where, for the theoretical calculations, correlation effects have been completely neglected. These differences displayed are almost identical, except these around the Γ' point (planes $P5$ and $P6$) where reconstructed densities strongly depend on the resolution. Supposing that they show smearing effects, in Fig. 10 we present the anisotropic parts of the densities, $\rho_a(\mathbf{p})=\rho(\mathbf{p})-\rho_0(p)$, for the pure theoretical EMD and for those reconstructed from both experimental and convoluted theoretical CP's. Now it is clear [see Fig. 10(a)] that the differences presented in Fig. 9 show smearing effects.

It is also seen that in spite of a large smearing of $\rho^{CP}(\mathbf{p})$, the overall behavior of the anisotropy is reproduced by the experiment (see also Fig. 8). This is the general trend observed in previous Compton scattering experiments:[27–31] The magnitude of the anisotropy is lowered by the e-e correlations. Due to this fact, we are sure that also in Y we observe strong e-e correlation effects. Because results presented in Fig. 9 are almost identical for positron annihilation and Compton scattering experiment, it seems that the correlation effect in these two experiments is similar [compare also results in Figs. 4(a) and 4(c)], even though in the Compton scattering data we could have only e-e correlations and not both e-e and e-p correlations as in the positron annihilation data.[38] However, our previous considerations showed that in the case of Y the e-p correlations do not change the momentum dependence of $\rho(\mathbf{p})$ in comparison with IPM; i.e., they can be neglected when absolute values of densities cannot be estimated.[39] Of course, this argument is not valid in the case of lifetime experiments where absolute values of the total probability of the positron annihilation are measured.[40]

So the final conclusion of all considerations is the following: in the Compton scattering experiment we observe e-e correlation effects which (i) decrease electron momentum densities at low momenta and (ii) introduce an additional smearing around $\mathbf{p}_F=\mathbf{k}_F+\mathbf{G}$, where $\mathbf{G}$ denotes a reciprocal lattice vector. The latter (smearing) effect, similar to the effect caused by a finite experimental resolution function, is observed also in 2D ACAR data. Here we would like to point out that a similar behavior of the e-p densities was observed by Manuel *et al.*[42] for Li, Al, and γ-Sn.

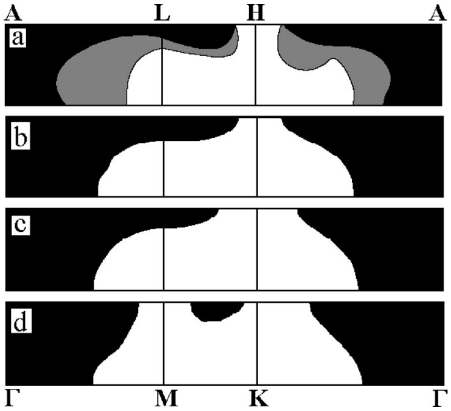

FIG. 11. Densities $\rho(\mathbf{k})$ in Y, on chosen symmetry planes for Loucks' theory (a), where values of $n_{\mathbf{k}}=0$, 1, and 2 are marked by black, grey, and white colors, respectively. $\rho^{dec}(\mathbf{k})$ (b), $\rho^{raw}(\mathbf{k})$ (c), and $\rho^{CP}(\mathbf{k})$ (d), marked by two colors, show the average FS's.

For the analysis of the FS (representing occupancy in $\mathbf{k}$ space) we applied the Lock-Crisp-West (LCW) (Ref. 13) procedure by folding the equivalent points in the extended momentum space $\mathbf{p}$ back into the first BZ (reduced $\mathbf{k}$ space),

$$\rho(\mathbf{k})=\sum_{\mathbf{G}}\rho(\mathbf{p}=\mathbf{k}+\mathbf{G})=\sum_j n_{\mathbf{k}j}=n(\mathbf{k}), \tag{14}$$

where the summation is over the reciprocal lattice vectors $\mathbf{G}$ and, for electronic densities, $n(\mathbf{k})$ denotes the number of occupied bands at the point $\mathbf{k}$. After conversion from $\mathbf{p}$- to $\mathbf{k}$-space lattice effects are emphasized, contributions of fully occupied bands should be constant and we can observe only contours of FS's.

In the case of experimental $\rho^{CP}(\mathbf{k})$ the LCW folding has been carried out over a cube in momentum space of sides 2 a.u. which involves 55 reciprocal vectors $\mathbf{G}$. The summation was performed in steps using successive groups of vectors $\mathbf{G}$, grouped according to their length. The procedure was convergent with increasing number of $\mathbf{G}$ up to 37, where $|\mathbf{G}|\leqslant 1.74$ a.u. (next $\mathbf{G}$ produce only undesirable fluctuations due to experimental errors).

To get LCW-folded densities $\rho^{raw}(\mathbf{k})$ and $\rho^{dec}(\mathbf{k})$ (shown in Fig. 11) we used a much higher number of $\mathbf{G}$ to obtain the FS of yttrium. Due to the fact that two FS's in yttrium are close to each other and because of smearing of the experimental $\rho(\mathbf{p})$, in Figs. 11(b)–11(d), we drew only the average FS's of the third and fourth bands.

LCW densities obtained from Compton and 2D ACAR experiments are essentially different. This is mainly due to the lower statistical accuracy of the Compton data and the second integration in momentum space. As we have already stated in our paper on $\mathrm{Cu_{0.9}Al_{0.1}}$,[26] it is clear that here one

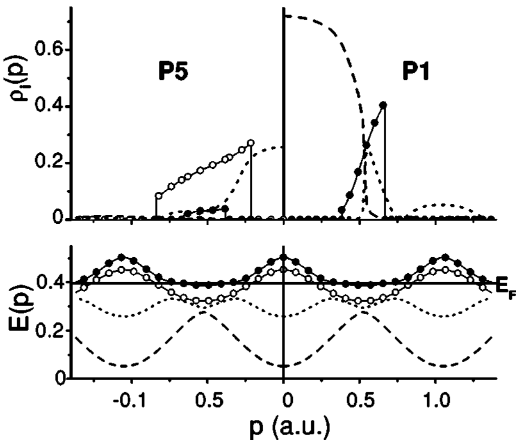

FIG. 12. Theoretical momentum densities in Y, $\rho_i(\mathbf{p})$, along ΓM on the first basal plane $P1$ and on the parallel plane $P5$ (defined in Fig. 2) with corresponding energy bands. Contributions from different valence bands i are marked by dashed $(i=1)$ and dotted $(i=2)$ lines and by open $(i=3)$ and solid $(i=4)$ circles.

would need a better statistics and resolution (at least 0.1 a.u.) in order to reach sufficient accuracy.

Finally, we demonstrate how the knowledge of $\rho(\mathbf{p})$ in the whole momentum space $\mathbf{p}$ gives us a possibility of obtaining some details of the FS via so-called symmetry selection rules.[11] Namely, due to the factor $e^{-i\mathbf{p}\cdot\mathbf{r}}$ in the expression for $\rho(\mathbf{p}=\mathbf{k}+\mathbf{G})$ [Eq. (13)], for a chosen $\mathbf{k}$, it depends on $\mathbf{G}$ which bands contribute to the momentum density.[16] E.g., in Fig. 12, let us consider $\rho(\mathbf{p})$ along the direction ΓM on the first ΓMK plane $(P1)$ and on the equivalent $\Gamma' M' K'$ $(P5)$. Despite the fact that on these two planes the energy $E(\mathbf{k})$ and thus also the occupation numbers $n_{\mathbf{k}j}$ are exactly the same, the $\rho_i(\mathbf{p})$ are quite different.

In the extended zone scheme $\rho(\mathbf{p})$ contains contributions from all states, i.e., also from the first two fully occupied valence bands which have the main contribution to $\rho(\mathbf{p})$ within the two first Brillouin zones. The third valence band [it does not contribute to $\rho(\mathbf{k}+\mathbf{G})$ for $\mathbf{G}=0$] causes a hole pocket around the Γ point: this feature starts to be visible around the $\Gamma' M' K'$ plane. Meanwhile, the fourth band has a dominant contribution on the ΓMK plane outside the first BZ. Due to such properties of $\rho(\mathbf{p})$, we were able to determine Fermi momenta $\mathbf{k}_F$ (marked by open circles in Fig. 2) from the 2D ACAR experiment (using the reconstructed densities for both raw and deconvoluted spectra[11]) but only for these values $\mathbf{k}_F$, for which densities $\rho(\mathbf{p})=\Sigma_i \rho_i(\mathbf{p})$ have a significant jump. It is seen that our results (within the experimental resolution) are in good agreement with theoretical calculations, marked by black dots.

From the Compton scattering data we were able to establish the Fermi momentum only on the first basal ΓMK plane along ΓM where there is a large jump of the density. Drawing the second derivative of $\rho^{CP}(\mathbf{p})$ (Fig. 13) we obtained $\mathbf{p}_F=0.66$ a.u., which is lower than the theoretical value of $\mathbf{p}_F=0.669$.

The same procedure applied to both ρ^{raw} and ρ^{dec} allowed to get $\mathbf{p}_F=0.68$ a.u. which is higher by 0.01 a.u. than the theoretical $\mathbf{p}_F$ and exactly the same as obtained in Ref. 11. Here $\mathbf{k}_F=2|\Gamma M|-\mathbf{p}_F$.

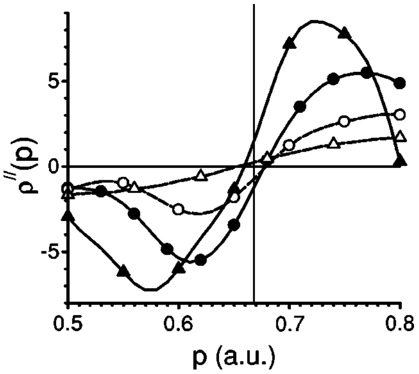

FIG. 13. Second derivative of densities in Y along ΓM on the $P1$ plane for $\rho^{dec}(p)$ and $\rho^{raw}(p)$ (solid and open circles, respectively) and $\rho^{CP}_{60}(p)$ and $\rho^{CP}_{36}(p)$ (solid and open triangles, respectively). Theoretical $\mathbf{p_F}=0.669$ a.u. is marked by the thin line.

IV. SUMMARY

The electron momentum density in Y, reconstructed from experimental high-resolution CP's, has been compared with *e-p* momentum densities reconstructed from 2D ACAR spectra and obtained via theoretical APW calculations. Both experiments show exactly the same shape of the anisotropy of the momentum densities $\rho(\mathbf{p})$, in agreement with the theory. A simultaneous analysis of both reconstructed densities and 1D profiles for these two experiments allows us to state that *e-e* correlation effects in Y are seen not only in the Compton scattering experiment but also in the ACAR data.

As we know from extensive theoretical investigations of the homogeneous electron gas,[32–36] such *e-e* correlation effects influence the EMD by an increased smearing of the FS and by the appearence of a momentum tail above the Fermi momentum k_F. Both effects have been frequently observed in CP experiments.

In the case of 2D ACAR measurements, we have both *e-e* and *e-p* correlations, and we learn from a fundamental paper by Carbotte and Kahana[38] that—at least for positrons in jellium—*the dynamical parts* of the *e-p* correlation effectively cancel the *e-e* correlation. Consequently, (almost) no tail beyond k_F should be observed in the *e-p* momentum density, and the remaining influence of fermion-fermion correlations comes from the *static* part of the *e-p* interaction, leading to a significant and strongly momentum-dependent increase of the *e-p* pair momentum density below k_F, an effect which we call the electron-positron rate (or *Kahana-like*) *enhancement*. However, Carbotte and Kahana's argumentation is only a qualitative one, and it is based on investigations of *jellium*. Beyond that, there exists another important theory by Arponen and Pajanne[41] about the behavior of a positron in an interacting electron gas which is represented by a system of Sawada bosons. The advantage of this procedure is that already the noninteracting bosons describe the electron-electron interaction on the level of the well-known *random phase approximation* (RPA), and each boson-boson interaction included into the theory goes beyond the RPA. Applying this approach on jellium, Arponen and Pajanne observed a significant tail of the electron-positron momentum density beyond k_F, in strong contradiction to the result of Ref. 38. Therefore, in ACAR spectra, a tail above the Fermi momentum cannot be excluded, especially not for real metals where the crystal potential causes a more or less strong *nonjellium* behavior of the electron gas.

According to our knowledge, the existence of such tails in positron annihilation data has been observed for the first time by Manuel *et al.*[42] for γ-Sn and even for such *jelliumlike* metals as Li and Al. Next, Ohata *et al.*[43] compared a high-resolution Compton profile of Al with a 1D ACAR spectrum along [111] direction. Their analysis leads to the following conclusions: the existence of a *Kahanalike* enhancement near the FS and a weaker tail for $p > p_F$ in the case of the 1D ACAR data compared to the CP's, as a result of the partial cancellation of e-e and e-p correlations.

We would like to point out that the BML theory, applied to Al,[44] gives the following results. Whereas the enhancement factor for momenta $p \leqslant p_F$ is similar to the *Kahanalike* enhancement, for $p > p_F$ the e-p interaction mainly decreases the contribution of umklapp components. Moreover, it reduces (in comparison with the IPM) the core contribution as well as the enhancement factor for core electrons decreases for higher momenta. So a weaker tail for $p > p_F$, observed in Al,[43] could be connected with these e-p correlation effects (not with weaker e-e correlations following from the theory[38]).

Therefore, in the case of a transition metal like Y, strong lattice effects have to be expected, and two of them can be clearly observed in the results of the present investigation: (i) We do not see any *Kahanalike* enhancement with its typically strong momentum dependence (see also Ref. 23), and (ii) there is only (if any) a very weak canceling between e-e and e-p correlation effects, and momentum components beyond k_F due to e-e interaction become clear visible.

Finally, knowledge of the symmetry selection rules has allowed us to establish values of some Fermi momenta.

ACKNOWLEDGMENTS

The authors would like to thank Dr. David Fort, University of Birmingham, U.K. for the original Y single crystals. We acknowledge the European Synchrotron Radiation Facility for providing synchrotron radiation facilities and we would like to thank Dr. Marco di Michiel and Dr. Thomas Buslaps for assistance in using the beam line ID15B. The work of Finland group was supported by the Academy of Finland (Grant Nos. 73759/40732/39182).

APPENDIX

The Radon transform[45] of the N-dimensional function $\rho(\mathbf{p})$ represents its integrals over $(N-1)$-dimensional hyperplanes:

$$g(r,\boldsymbol{\zeta}) = \int_{-\infty}^{\infty} \rho(\mathbf{p})\,\delta(r-\boldsymbol{\zeta}\cdot\mathbf{p})\,d\mathbf{p}. \tag{A1}$$

Here $r=\boldsymbol{\zeta}\cdot\mathbf{p}$ defines this hyperplane where $\boldsymbol{\zeta}$ is a unit vector in $\mathcal{R}^N$ along r and r is a perpendicular distance of the hyperplane from the origin of the coordinate system. Here vector $\mathbf{p}$ is described by $p=|\mathbf{p}|$ and $\boldsymbol{\omega}$ (e.g. Ref. 46).

Both functions g and ρ can be expanded into spherical harmonics of degree l, S_l, defined in $\mathcal{R}^N$:

$$g(r,\boldsymbol{\zeta}) = \sum_l g_l(r) S_l(\boldsymbol{\zeta}), \tag{A2}$$

$$\rho(p,\boldsymbol{\omega}) = \sum_l \rho_l(p) S_l(\boldsymbol{\omega}). \tag{A3}$$

Deans[46] showed that the radial functions g and ρ are the Gegenbauer transform pair, where

$$\rho_l(p) = c\,\frac{1}{p}\int_p^{\infty} g_l^{(2\mu+1)}(r)\,C_l^{\mu}(q)\,[q^2-1]^{\mu-1/2}\,dr, \tag{A4}$$

with

$$c = \frac{(-1)^{2\mu+1}}{2\pi^{\mu+1}}\,\frac{\Gamma(l+1)\Gamma(\mu)}{\Gamma(l+2\mu)}.$$

Here $g^{(n)}$ denotes the nth derivative of g; C_l^{μ} are Gegenbauer polynomials, $q=r/p$, and $\mu=N/2-1$.

This equation can be solved analytically as done by Louis.[47] Choosing $\lambda=N/2$ we obtain

$$g_l(r) = \sum_{k=0}^{\infty} a_{lk}(1-r^2)^{N/2-1/2}\,C_{l+2k}^{N/2}(r), \tag{A5}$$

$$\rho_l(p) = \sum_{k=0}^{\infty} a_{lk}\,b\,p^l\,P_k^{(0,l+N/2-1)}(2p^2-1). \tag{A6}$$

Here $P_k^{(a,b)}$ are Jacobi polynomials and the coefficients b are defined as

$$b = 2^{1-N}\pi^{1-N/2}\,\frac{\Gamma(l+2k+N)}{\Gamma(l+2k+1)\Gamma(N/2)}.$$

For $N=2$ and knowing that

$$C_n^1(x) = U_n(x), \qquad x^n P_m^{(0,n)}(2x^2-1) = R_n^m(x),$$

one gets reconstruction algorithm for line integrals. For $N=3$ and knowing that

$$C_n^{3/2}(x) = \frac{\Gamma(n+3)\Gamma(2)}{\Gamma(n+2)\Gamma(3)}\,P_n^{(1,1)}(x) = \frac{n+2}{2}\,P_n^{(1,1)}(x),$$

one obtains reconstruction algorithm for plane integrals, both described in the Sec. II B.

Another analytical solution (also in $\mathcal{R}^N$ but in terms of orthogonal Hermite and Laguerre polynomials) was derived by Cormack.[48] Of course, there is also a lot of other reconstruction techniques based on, e.g., Fourier transform methods—for more details see, e.g., Refs. 15, 16, and 46.

[1] T. L. Loucks, Phys. Rev. **144**, 504 (1966).

[2] S. Altmann and C. J. Bradley, Proc. Phys. Soc. London **92**, 764 (1967).

[3] H. L. Skriver and A. R. Mackintosh, in *Physics of Transition Metals*, edited by P. Rhodes, Inst. Phys. Conf. Series No. 55 (Institute of Physics, Bristol, 1980), p. 29.

[4] G. Y. Guo, W. M. Temmerman, and Z. Szotek, Newsletter, **13**, 14 (1989).

[5] M. Matsumoto, J. B. Staunton, and P. Strange, J. Phys.: Condens. Matter **3**, 1453 (1991).

[6] A. M. Begeley, Ph.D. thesis, University of Birmingham, 1990; A. M. Begeley and W. Temmerman (unpublished).

[7] R. W. Williams, T. L. Loucks, and A. R. Mackintosh, Phys. Rev. Lett. **16**, 168 (1966).

[8] R. W. Williams and A. R. Mackintosh, Phys. Rev. **168**, 679 (1968).

[9] R. P. Gupta and T. L. Loucks, Phys. Rev. **176**, 848 (1968).

[10] S. B. Dugdale, H. M. Fretwell, M. A. Alam, G. Kontrym-Sznajd, R. N. West, and S. Badrzadeh, Phys. Rev. Lett. **79**, 941 (1997).

[11] G. Kontrym-Sznajd, H. Sormann, and R. N. West, Mater. Sci. Forum **363-365**, 558 (2001).

[12] P. G. Mattocks and R. C. Young, J. Phys. F: Met. Phys. **8**, 1417 (1978).

[13] D. G. Lock, V. H. C. Crisp, and N. R. West J. Phys. F: Met. Phys. **3**, 561 (1972).

[14] R. Harthoorn and P. E. Mijnarends, J. Phys. F: Met. Phys. **8**, 1147 (1978).

[15] G. Kontrym-Sznajd and M. Samsel-Czekała, Appl. Phys. A: Mater. Sci. Process. **70**, 89 (2000); G. Kontrym-Sznajd, M. Samsel, and R. N. West, Acta Phys. Pol. A **95**, 591 (1999).

[16] A. M. Cormack, J. Appl. Phys. **35**, 2908 (1964); G. Kontrym-Sznajd, Phys. Status Solidi A **117**, 227 (1990).

[17] G. Kontrym-Sznajd, A. Jura, and M. Samsel-Czekała, Appl. Phys. A: Mater. Sci. Process. **74**, 605 (2001).

[18] P. Suortti, T. Buslaps, P. Fajardo, V. Honkimäki, M. Kretzschmer, U. Lienert, J. E. McCarthy, M. Renier, A. Shukla, Th. Tschentscher, and T. Meinander, J. Synchrotron Radiat. **6**, 69 (1999).

[19] R. N. West, in *Positron Spectroscopy of Solids*, edited by A. Dupasquier and A. P. Mills, Jr. (IOS Press, Amsterdam, 1995).

[20] S. B. Dugdale, M. A. Alam, H. M. Fretwell, M. Biasini, and D. Wilson, J. Phys.: Condens. Matter **6**, L435 (1994); H. M. Fretwell, S. B. Dugdale, M. A. Alam, M. Biasini, L. Hoffmann, and A. A. Manuel, Europhys. Lett. **32**, 771 (1995).

[21] M. Biasini (private communication); U. Gerhardt, S. Marquardt, N. Schroder, and S. Weiss, Phys. Rev. B **58**, 6877 (1998), and references therein.

[22] H. Sormann, Phys. Rev. B **43**, 8841 (1991).

[23] H. Sormann, G. Kontrym-Sznajd, and R. N. West, Mater. Sci. Forum **363-365**, 609 (2001); H. Sormann (unpublished).

[24] D. A. Cardwell and M. J. Cooper, J. Phys.: Condens. Matter **1**, 9357 (1989).

[25] L. Lam and P. M. Platzman, Phys. Rev. B **9**, 5122 (1974).

[26] M. Samsel-Czekała, G. Kontrym-Sznajd, G. Döring, W. Schülke, J. Kwiatkowska, F. Maniawski, S. Kaprzyk, and A. Bansil, Appl. Phys. A (to be published).

[27] G. Stutz, F. Wohlert, A. Kaprolat, W. Schülke, Y. Sakurai, Y. Tanaka, M. Ito, H. Kawata, N. Shiotani, S. Kaprzyk, and A. Bansil, Phys. Rev. B **60**, 7099 (1999), and references therein.

[28] Y. Tanaka, Y. Sakurai, A. T. Stewart, N. Shiotani, P. E. Mijnarends, S. Kaprzyk, and A. Bansil, Phys. Rev. B **63**, 045120 (2001).

[29] W. Schülke, G. Stutz, F. Wohlert, and A. Kaprolat, Phys. Rev. B **54**, 14 381 (1996).

[30] S. Huotari, K. Hämäläinen, S. Manninen, S. Kaprzyk, A. Bansil, W. Caliebe, T. Buslaps, V. Honkimäki, and P. Suortti, Phys. Rev. B **62**, 7956 (2000).

[31] J. A. Soininen, K. Hämäläinen, and S. Manninen, Phys. Rev. B **64**, 125116 (2001).

[32] E. Daniel and S. Vosko, Phys. Rev. **120**, 2041 (1960).

[33] J. Lam, Phys. Rev. B **3**, 3243 (1971).

[34] A. W. Overhauser, Phys. Rev. B **3**, 1888 (1971).

[35] L. J. Lantto, Phys. Rev. B **22**, 1380 (1980).

[36] Y. Takada and H. Yasutami, Phys. Rev. B **44**, 7879 (1991).

[37] Because of the noise in CP's [see also Fig. 4(c)], reconstructed densities $\rho^{CP}(\mathbf{p})$ had to be additionally smeared within the reconstruction procedure (Ref. 15) by using a small number of orthogonal polynomials in the expansion [Eq. (6)]. This is not the case for either $\rho^{dec}(\mathbf{p})$ or $\rho^{raw}(\mathbf{p})$, which were described within Cormack's method (Ref. 16) by a high number of orthogonal polynomials in Eq. (10).

[38] J. P. Carbotte and S. Kahana, Phys. Rev. **139**, A213 (1965).

[39] In the case of the ACAR data we do not measure the absolute value of the momentum density $\rho(\mathbf{p})$. Due to the presence of the positron, the normalization of the spectra is somewhat ambiguous, contrary to the Compton spectra, where the area of the Compton profile equals the number of valence electrons. In the case of the CPs, after their normalization, we obtained lower values of densities for low momenta in comparison with the theoretical density [compare Figs. 5(a) and 5(c)] what was attributed to e-e correlations. Due to this reasons, in order to compare the momentum dependence of theoretical results to the experimental ones in the same way for both CP and 2D ACAR data, we renormalized all densities to the same value at $p=0$.

[40] S. Daniuk, M. Šob, and A. Rubaszek, Phys. Rev. B **43**, 2580 (1991).

[41] J. Arponen and E. Pajanne, Ann. Phys. (N.Y.) **121**, 343 (1979); J. Phys. F: Met. Phys. **9**, 2359 (1979).

[42] A. A. Manuel, D. Vasumathi, B. Barbiellini, A. Shukla, P. Suortti, and T. Chiba, Mater. Sci. Forum **255-257**, 760 (1997).

[43] T. Ohata, M. Itou, I. Matsumoto, Y. Sakurai, H. Kawata, N. Shiotani, S. Kaprzyk, P. E. Mijnarends, and A. Bansil, Phys. Rev. B **62**, 16 528 (2000).

[44] H. Sormann, Phys. Rev. B **54**, 4558 (1996).

[45] J. Radon, Ber. Verh. Sachs. Akad. **69**, 262 (1917).

[46] S. R. Deans, *The Radon Transform and Some of Its Applications* (Wiley, New York, 1983).

[47] A. K. Louis, SIAM (Soc. Ind. Appl. Math.) J. Math. Anal. **15**, 621 (1984).

[48] A. M. Cormack, Proc. Am. Math. Soc. **86**, 293 (1982).